Supplementary Information for "Driven transport of dilute polymer solutions through porous media comprised of interconnected cavities"

1. Mathematical Expressions for inter-particle DPD forces

The position and velocity vectors of particles *i* and *j* are denoted by $\mathbf{r}_i$, $\mathbf{v}_i$, $\mathbf{r}_j$ and $\mathbf{v}_j$ respectively. Furthermore, $\mathbf{r}_{ij} = \mathbf{r}_i - \mathbf{r}_j$, $\mathbf{v}_{ij} = \mathbf{v}_i - \mathbf{v}_j$, $r_{ij} = |\mathbf{r}_{ij}|$ and $\hat{\mathbf{r}}_{ij} = \mathbf{r}_{ij}/r_{ij}$. The conservative force is expressed as

$$\mathbf{F}_{ij}^{C} = \begin{cases} a_{ij}(1 - r_{ij})\hat{\mathbf{r}}_{ij}, & r_{ij} < 1 \\ \mathbf{0}, & \text{otherwise} \end{cases} \quad \text{(S1)}$$

where a_{ij} is the maximum repulsive force between particles *i* and *j*. The dissipative and random forces are expressed as

$$\mathbf{F}_{ij}^{D} = -\gamma w^{D}(r_{ij})(\hat{\mathbf{r}}_{ij} \cdot \mathbf{v}_{ij})\hat{\mathbf{r}}_{ij}, \quad \mathbf{F}_{ij}^{R} = \sigma w^{R}(r_{ij})\zeta_{ij}\Delta t^{-1/2}\hat{\mathbf{r}}_{ij} \quad \text{(S2)}$$

where w^D and w^R are weighting functions that vanish for $r_{ij} > 1$ and ζ_{ij} is a Gaussian random number with zero mean and unit variance. The fluctuation-dissipation theorem requires that $w^D(r)$ and $w^R(r)$, as well as γ and σ, are related according to

$$w^{D}(r) = [w^{R}(r)]^2, \quad \sigma^2 = 2\gamma k_B T\,. \quad \text{(S3)}$$

In this study, $w^D(r)$ and $w^R(r)$ are expressed as

$$w^{D}(r) = [w^{R}(r)]^2 = \begin{cases} (1 - r)^2 & r < 1 \\ 0 & r \geq 1 \end{cases}. \quad \text{(S4)}$$

The above expressions were used when evaluating inter-particle forces for interactions not involving wall beads. For such interactions, the coefficients γ and σ that appear in the expressions for $\mathbf{F}_{ij}^{D}$ and $\mathbf{F}_{ij}^{R}$ in equation (S2) were replaced by γ_e and σ_e, whose values depend upon ϕ_i according to equations 6 and 12 of Li et al.'s paper[1].

2. Effect of simulation box size

To check for finite size effects, the flow case with $F_e = 0.14$ was simulated using a box of side length 40. For this test run, linear polymers with N = 73 were used because they have the largest equilibrium radius of gyration amongst all the different polymer architectures and chain lengths investigated. The results are compared in Table S1. Here, $G_{\alpha\beta}^2$ denotes the αβ components of the gyration tensor averaged over all chains and the simulation time while *v* denotes the average velocity of the polymers' center of mass (COM). The side length of the cubic simulation box is denoted as *L*. The results for $G_{\alpha\beta}^2$ and *v* are observed to be very similar

for the two cases, indicating that the choice of L = 20 used in this study is sufficiently large so as to avoid finite size effects.

Table S1. Comparison of results for different side lengths of the simulation box, L.

	G_{xx}^2	$(G_{yy}^2 + G_{zz}^2)/2$	v
L = 20	9.14 ± 0.25	1.76 ± 0.06	0.44 ± 0.01
L = 40	9.23 ± 0.16	1.77 ± 0.02	0.43 ± 0.01

3. Velocity profile

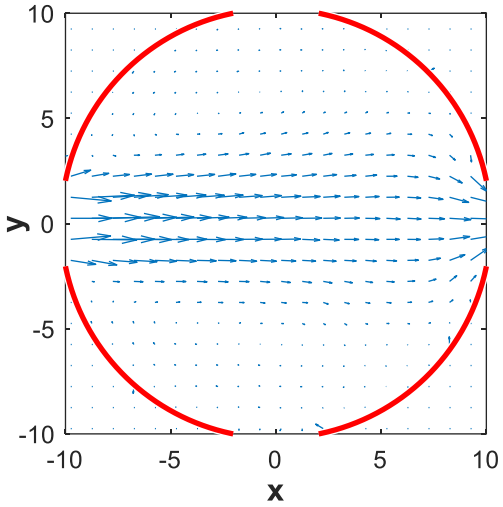

Figure S1. Velocity profile for pressure-driven flow of pure solvent through the cavity array shown in Figure 1 of the main text. The value of F_e is 0.14.

The velocity profile within the cavity for the case of pressure-driven flow of pure solvent in the absence of the polymer is shown in Figure S1 for F_e = 0.14. The results indicate that the flow remains laminar for the largest value of F_e tested. For F_e = 0.14, the average magnitude of velocity in the cavity is found to be 0.41. For the parameter settings used in this study, the kinematic viscosity of the fluid in the absence of the polymer is estimated to be 0.27[2]. Hence, Re is estimated as $Re = \frac{UR_c}{\eta_k} = 15.5$, where U, R_c and η_k denote the characteristic velocity, cavity radius and kinematic viscosity respectively.

4. Effect of HI

For the flow case, additional simulations were performed without hydrodynamic interactions (HI), as described in Section 2. The results indicate that these interactions mainly affect the extent to which the chain conformation is distorted by the flow and the extent of chain orientation along the

flow direction. Therefore, the results for R_f, R_p and $\langle\theta\rangle$ in the presence and absence of HI for linear, ring and star polymers are compared in this section. The values of N are 25, 37 and 73 for linear, ring and star polymers respectively. The values of $R_{g,e}$ in the absence of flow are similar for these 3 cases, ranging between 1.33 and 1.39.

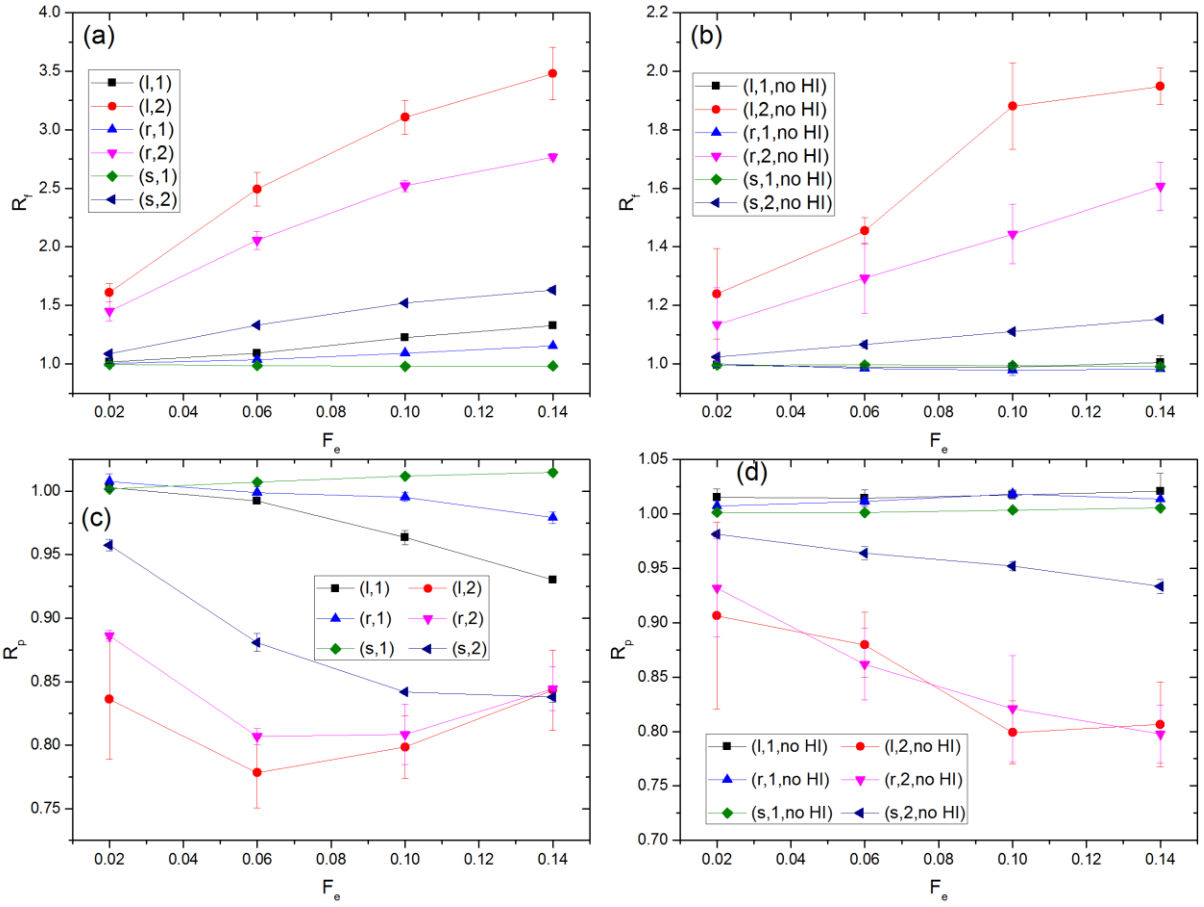

Figure S2. Effect of varying F_e upon (a) R_f with HI, (b) R_f without HI, (c) R_p with HI and (d) R_p without HI. The abbreviations, l, r and s denote linear, ring and star polymers with 12 arms respectively.

The values of R_f and R_p for simulations with and without HI for the 3 different polymer types are shown in Figure S2. The main observation is that the extent of increase in R_f and decrease in R_p with increasing F_e is greater in the presence of HI.

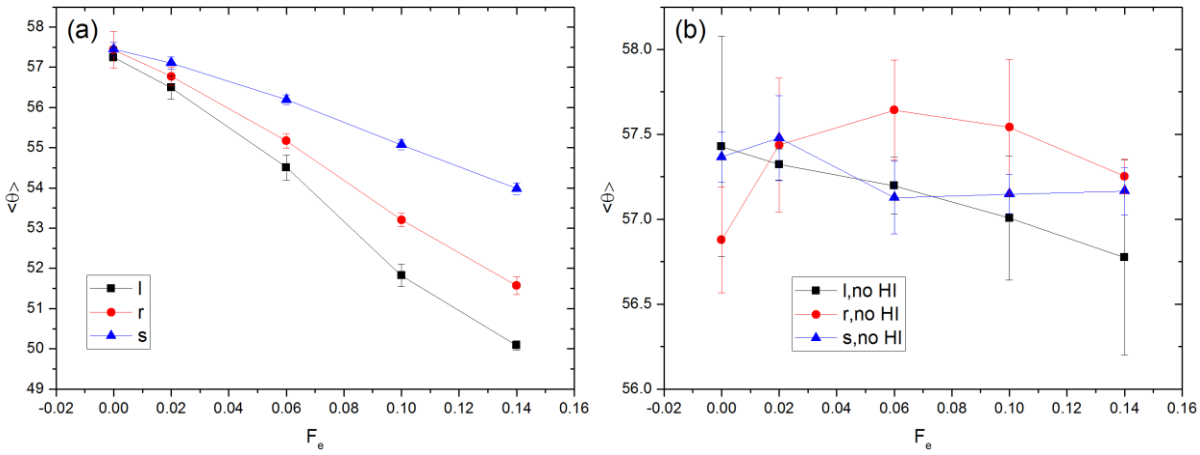

Figure S3. Angle between eigenvector corresponding to largest eigenvalue of gyration tensor and the flow direction (a) with HI and (b) without HI.

The effect of HI upon <θ> is illustrated in Figure S3. It is seen that <θ> decreases with increasing F_e in the presence of HI whereas no such trend is observed in their absence.

5. Alignment between polymers

As shown in Figures 4(a) and 8(b) of the main text, the polymers rotate so as to become aligned along the direction of the external force. The resultant increase in the extent of orientational order among the chains can be quantified by evaluating the principal orientational order parameter, which is defined as the eigenvalue of the Saupe order tensor with the largest magnitude[3]. This quantity is denoted as λ_{max} and its variation with F_e for the field and flow cases for linear polymers with N = 73 is shown in Figure S4. It is seen that λ_{max} increases with F_e for both types of driving force. The extent of increase is greater for the flow as compared to the field case, in agreement with the results in Figure 4(a) of the main text.

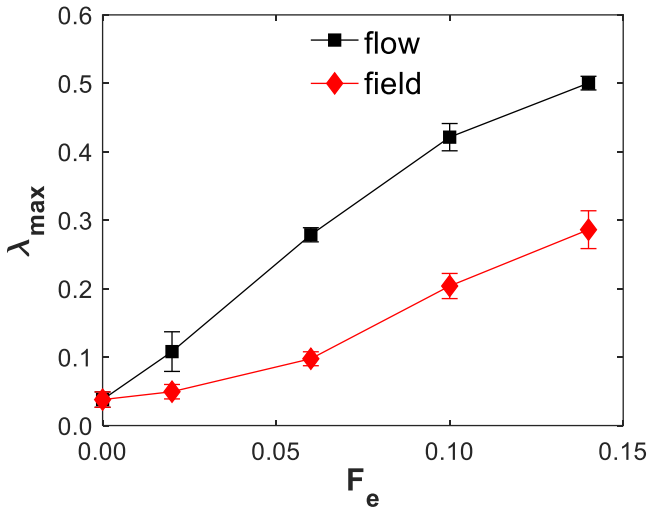

Figure S4. Variation of principal order parameter, λ_{max} with external force magnitude, F_e for field and flow cases. The results are for a linear polymer with N = 73.

6. Simulation Snapshots

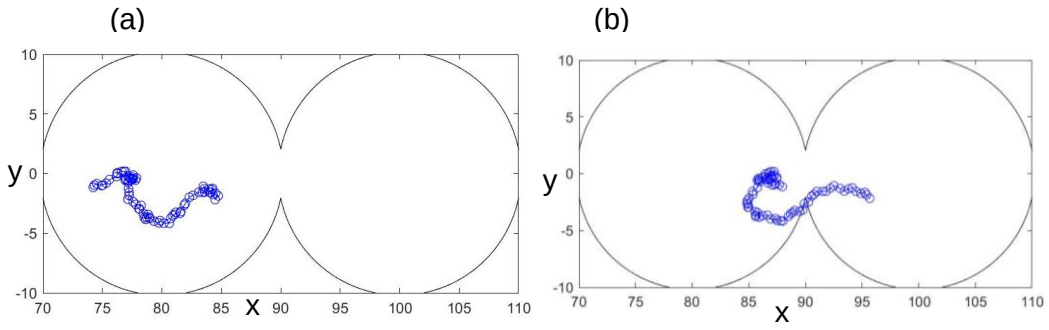

Figure S5. Simulation snapshots of a linear polymer occupying (a) one and (b) two cavities.

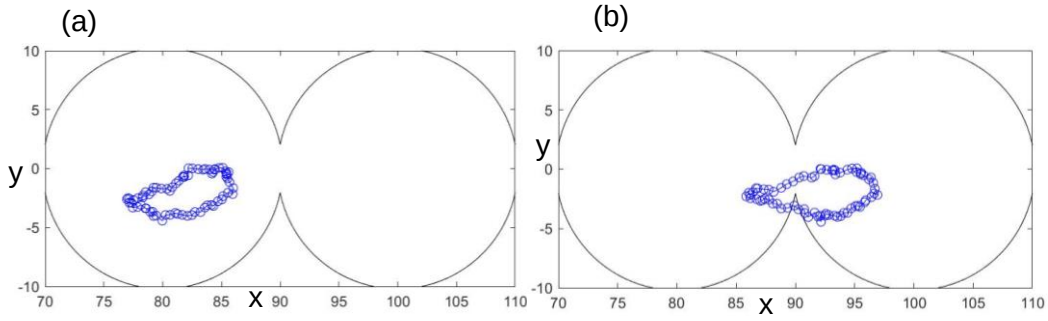

Figure S6. Simulation snapshots of a ring polymer occupying (a) one and (b) two cavities.

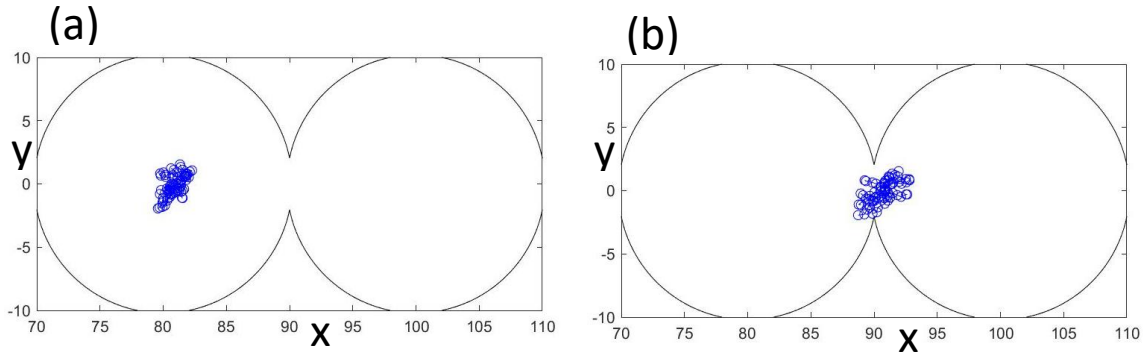

Figure S7. Simulation snapshots of a 12 arm star polymer occupying (a) one and (b) two cavities.

Representative simulation snapshots for the flow case with F_e = 0.14 and N = 73 are shown in Figure S5-Figure S7 for the 3 different polymer types.

7. Variation of $\langle\theta\rangle$ with F_e for different polymer types for the field case

The variation of $\langle\theta\rangle$ with F_e for linear, ring and star polymers for the field case are shown in Figure S8. The corresponding values of N are 25, 37 and 73 respectively. The equilibrium radius of gyration, $R_{g,e}$, is similar for these cases and ranges between 1.33 and 1.39. Unlike the flow case, for which the results are shown in Figure 8(b) of the main text, $\langle\theta\rangle$ hardly varies with F_e. This suggests that gradients in the solvent velocity field are responsible for the observed alignment of the eigenvector corresponding to the largest eigenvalue of gyration tensor along the direction of the external force.

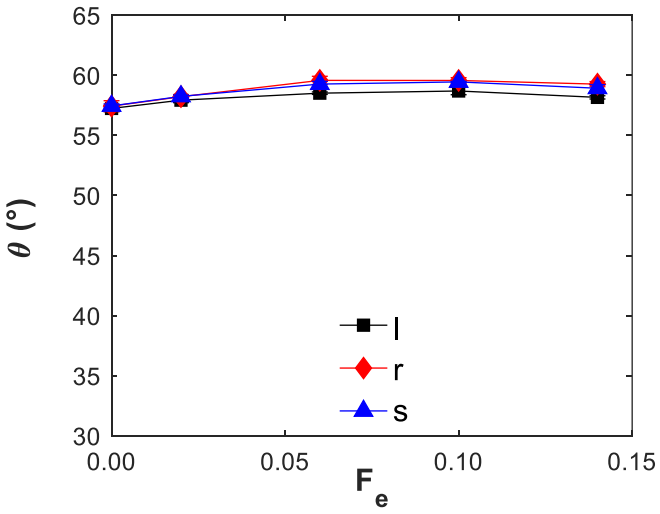

Figure S8. Variation of $\langle\theta\rangle$ with F_e for different polymer types. The labels l, r and s denote linear ring and star polymers with 12 arms respectively. The corresponding values of N are 25, 37 and 73.

8. Effect of external field orientation upon center of mass velocity

The values of the polymers' center of mass velocity, v, for the scenarios in which the external force acts along the x-direction and at a 45° angle with respect to the x-axis in the x-y plane for the field case were presented in the main text. The effect of external force direction upon v for the field case was further analyzed by performing additional simulations for which the angle between the external force vector and x-axis, ϕ, was set to 15° and 30°. The results are shown in Figure S9 for the case F_e = 0.14. The values of N for linear, ring and star polymers were set to 25, 37 and 73 respectively such that their radii of gyration are similar at equilibrium. It is seen that v decreases monotonically as ϕ increases because the polymers' motion along the field direction becomes increasingly hindered by the cavity walls. In addition, the difference in v between the different polymer types decreases as ϕ increases.

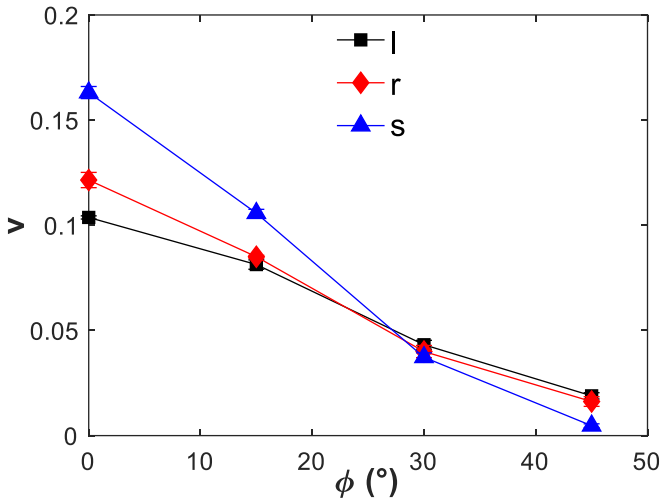

Figure S9. Effect of ϕ upon velocity of polymers' center of mass velocity along external field direction for the field case with F_e = 0.14. The labels l, r and s denote linear, ring and star polymers respectively. The corresponding values of N are 25, 37 and 73.

References

1. Li, Z.; Bian, X.; Tang, Y.H.; Karniadakis, G.E. A dissipative particle dynamics method for arbitrarily complex geometries. *J. Comput. Phys.* **2018**, *355*, 534–547, doi:10.1016/j.jcp.2017.11.014.

2. Fan, X.; Phan-Thien, N.; Chen, S.; Wu, X.; Ng, T.Y. Simulating flow of DNA suspension using dissipative particle dynamics. *Phys. Fluids* **2006**, *18*, 063102, doi:10.1063/1.2206595.

3. Topgaard, D. Director orientations in lyotropic liquid crystals: diffusion MRI mapping of the Saupe order tensor. *Phys. Chem. Chem. Phys.* **2016**, *18*, 8545–8553, doi:10.1039/C5CP07251D.